Observation of quantum dynamical oscillations of ultracold atoms in the *F* and *D* bands of an optical lattice

Zhongkai Wang (王中凯),[1] Baoguo Yang (杨保国),[1] Dong Hu (胡栋),[1] Xuzong Chen (陈徐宗),[1]
Hongwei Xiong (熊宏伟),[2] Biao Wu (吴飙),[2,3,4] and Xiaoji Zhou (周小计)[1,*]

[1]*School of Electronics Engineering and Computer Science, Peking University, Beijing 100871, China*
[2]*Wilczek Quantum Center, College of Science, Zhejiang University of Technology, Hangzhou 310014, China*
[3]*International Center for Quantum Materials, School of Physics, Peking University, Beijing 100871, China*
[4]*Collaborative Innovation Center of Quantum Matter, Beijing 100871, China*

(Received 29 September 2015; published 19 September 2016)

We report the observation of quantum dynamical oscillations of ultracold atomic gases in the *F* and *D* bands of an ordinary optical lattice. We are able to control the Bragg reflections at the Brillouin-zone edge up to the third order. As a result, we can switch the quantum dynamics from oscillations across both the *F* and *D* bands to oscillations only within the *F* band. Our capability to observe these oscillations comes from a nonadiabatic technique which allows us to load ultracold atoms efficiently to the *G* band of an optical lattice.

DOI: 10.1103/PhysRevA.94.033624

I. INTRODUCTION

There has been a lot of effort both experimentally and theoretically to study the quantum dynamics of ultracold atoms in an optical lattice (OL), such as the celebrated Bloch oscillations (BOs) [1–6] and the Landau-Zener (LZ) tunneling [3,7–10]. These studies have focused on the lowest band as it is hard to load atoms to high bands and then control their quantum dynamics experimentally. Recently, people have been pushing the boundary and studying quantum dynamics involving more than one band. The effort has resulted in the observation of Bloch-Zener oscillations (BZOs) [11–17], where the quantum oscillations are between two Bloch bands and the crossing between these two bands is facilitated by the LZ tunneling.

However, this kind of oscillation within two Bloch bands is very difficult to observe in a simple ordinary OL. In this kind of simple lattice, the band gaps are always smaller for higher bands. If atoms can tunnel from the *S* band to the *P* band, they should also be able to tunnel from the *P* band to the *D* band. As a result, the oscillations would involve uncontrollably many bands [18]. To control oscillations within two bands, one has to design lattices with more complex constructions, which include a binary lattice in waveguide arrays [14], the honeycomb lattice [15], and the miniband structure [16,17]. In this work we demonstrate experimentally that we can initiate and control quantum oscillations with two high excited bands in a simple ordinary OL, where the variable external force from the harmonic trap instead of the usual linear external potential is used.

In this work the Bose-Einstein condensate (BEC) is initially loaded nonadiabatically into the *G* band of a one-dimensional ordinary OL. It subsequently tunnels to the *F* band and begins oscillations within the *F* and *D* bands, which are clearly observed in the momentum space. We can control the Bragg reflection between momenta $3\hbar k_L$ and $-3\hbar k_L$, which is at the first Brillouin zone (FBZ) edge between the *F* and *D* bands, by tuning the OL strength. k_L is the wave vector of the laser forming the lattice. When the Bragg reflection is weak, quantum oscillations crossing the *F* and *D* bands are observed. When the reflection is strong, quantum oscillations are observed in only the *F* band. When the Bragg reflection is at intermediate strength, we observe the superposition of these two types of quantum oscillations. In our results, the oscillations crossing the two excited bands can last up to 58 ms, which is much longer than the BZOs observed in Ref. [17]. The long oscillation time is due to the small influence of interatomic two-body interaction in the higher-energy bands, which is smaller than the interaction in lower-energy bands. Therefore, the coherence can be kept for a long time, which is helpful to the interference experiment in precision measurement. During the oscillations, the BEC can be displaced up to ± 100 μm (470 lattice sites) in space, which is bigger than the spatial displacement observed in super-Bloch oscillations [6].

II. EXPERIMENTAL METHOD TO PREPARE THE ATOMS IN THE HIGH BANDS

In our experiment, a pure BEC of about 1.5×10^5 ^{87}Rb atoms is prepared in a hybrid trap which is formed by overlapping a single-beam optical dipole trap with a wavelength of 1064 nm and a quadrupole magnetic trap. The resulting harmonic trapping frequencies are $(\omega_x,\omega_y,\omega_z) = 2\pi \times (28,55,65)$Hz. After preparing a BEC in the harmonic trap, by using a series of standing-wave OL pulses within tens of microseconds [19,20], we load the BEC into the *G* band of a one-dimensional OL (along the *x* direction) at the quasimomentum $\hbar q = 0$. The OL is created by two counterpropagating laser beams with the lattice constant $a =$ 426 nm. The spatial potential is given by $V_0 \cos^2(k_L x)$, with V_0 being the lattice depth shown in Fig. 1(a).

This nonadiabatic shortcut method [19,20] consists of a series of standing-wave pulses, as shown in Fig. 1(a), where the pulse duration t_i and the interval t_{fi} ($i = 1,2,3,\ldots$) between pulses are drawn schematically and are not in proportion to the real time durations. The time t is the holding time of the BEC in the OL. It allows us to nonadiabatically load a BEC from the ground state of the harmonic trap $|\psi_0\rangle$ directly into a target state $|\psi_a\rangle = |n,q\rangle$. Here $|n,q\rangle$ is a Bloch state,

*xjzhou@pku.edu.cn

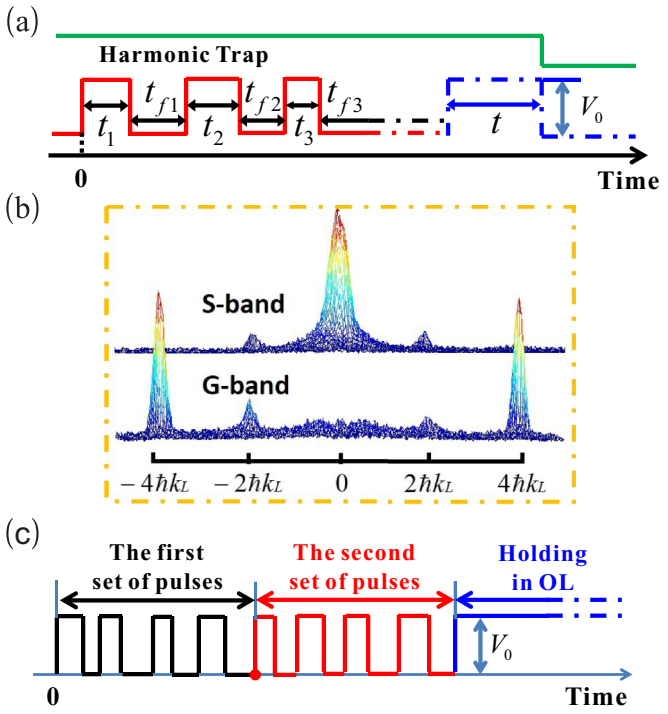

FIG. 1. (a) The time sequence for loading atoms into a target Bloch state $|n,q\rangle$ and the holding time t in the OL. (b) TOF pictures taken after loading atoms into the S and G bands. (c) A time sequence consists of two sets of pulses for loading atoms into the Bloch state in the F band with $q = 0$. Here eight pulses are shown, and in real experiments the number of pulses can vary for different purposes.

where $n = 1,2,3,\ldots$ is the band index corresponding to the S band, P band, D band, etc. The durations t_i and intervals t_{fi} of the standing wave series depend on the target state $|n,q\rangle$ and OL depth. The pulse sequence can be optimized so that the final state is nearly a Bloch state (the fidelity can be over 98%). For instance, for an OL depth of $7.5E_r$, by using the time sequence $(t_1,t_{f1},t_2,t_{f2},t_3,t_{f3},t_4,t_{f4},t_5,t_{f5},t_6,t_{f6}) = (20,40,42,14,14,12,14,12,20,4,22,34)$ μs, we obtain the Bloch state in the G band with $q = 0$. For the Bloch state in the G band with $q = 0$, $\pm 4\hbar k_L$ momentum components have dominant populations, while $0\hbar k_L$ dominates for the Bloch state in the S band with $q = 0$, as shown by the experimental results in Fig. 1(b) for $V_0 = 5E_r$. To get the Bloch state in the F band with $q = 0$, because of the odd parity, we need two sets of standing-wave pulses [21], as shown in Fig. 1(c). Starting from the plane wave with zero momentum, in the first set of pulses, the atoms experience spatial potential $V_0\cos^2(k_L x)$, during which atoms distribute in the even-parity bands, such as the S and D bands. For the second set of pulses, the atoms experience spatial potential $V_0\cos^2(k_L x+3\pi/4)$, during which atoms distribute in the odd-parity bands, such as the P and F bands. For convenience, we load atoms into the G band, with pulses only including potential $V_0\cos^2(k_L x)$ in the experiment.

III. EXPERIMENTAL OBSERVATION

After the BEC in the G band is prepared, we hold the lattice and harmonic trap for a period of time t and then switch off all potentials to take pictures after a 28-ms time of flight (TOF). Three series of experimental absorption images for the OL depths $V_0 = 5E_r$, $7.5E_r$, and $15E_r$ are shown, respectively, in Figs. 2(a)–2(c). $E_r = \hbar^2 k_L^2/2m$ is the recoil energy, with m being the atomic mass. The time separation between neighboring images in the $5E_r$ series is 1 and 0.5 ms in the other two series. These series of images demonstrate clearly three different quantum oscillations; we will explain and analyze them later. For convenience, an extended band structure is drawn in Fig. 2(d), where the energy gaps between different bands are marked with A_s ($s = 1,2,3,4,5,6$).

The BEC is initially loaded in the G band, where the atoms mostly populate equally around two momenta $\pm 4\hbar k_L$. As atoms with these two momenta are at the center of the trapping potential at the beginning, the only possible motion for them is to move either to the left or the right. Consequently, they lose their momenta while gaining harmonic potential energy. This corresponds to the BEC quantum tunneling from the G band to the F band over the tiny band gap at A_1 and A_6 in Fig. 2(d). It is impossible for the BEC to move up along the G band due to the conservation of energy. When the lattice depth is very high and, as a result, the energy gap at A_1 and A_6 is large, it is possible for the BEC to stay in the G band for a long time. We have observed atoms remaining in the G band for 5 ms when $V_0 = 20E_r$. For the lattice strength of interest in our experiment, the BEC always tunnels from the G band to the F band as soon as the initial loading ends.

Once the BEC is in the F band, it continues to lose momentum while gaining harmonic potential energy. This corresponds to the BEC traversing dynamically along the F band from A_1 and A_6 to A_2 and A_5 in Fig. 2(d). Once arriving at A_2 and A_5, the atoms face different ensuing dynamics depending on the lattice strength. If the lattice strength is small and the Bragg reflection at A_2 and A_5 is weak, the BEC will continue its dynamics into the D band by crossing the band gap. After evolving dynamically along the entire D band, the BEC comes to the band gap between the D and P bands at A_3 and A_4. This band gap is always large for the lattice strength in our experiments. As a result, the atoms at A_3 ($-2\hbar k_L$) will be Bragg reflected completely to A_4 ($2\hbar k_L$), while the atoms at A_4 will be Bragg reflected completely to A_3. No tunneling to the P band occurs. Afterwards, the BEC will reverse its dynamics by moving up in momentum from A_4 and A_3 to A_5 and A_2. It eventually arrives at A_6 and A_1, finishing half of an oscillating cycle. These oscillations crossing the two Bloch bands (F and D bands) are driven under a variable force from the harmonic trap. They are illustrated in Fig. 2(a) for lattice depth $V_0 = 5E_r$, and their period is 24 ms.

Note that the BEC moving up along the bands around A_4 and A_3 in Fig. 2(d) by gaining momenta is due to the fact that most of the atoms are away from the center of the trapping potential and feel an accelerating force. This is different from the initial stage when the BEC is loaded into the G band, where most of the atoms are at the center of the trap and feel a very small force for the finite size of the BEC.

When the OL is strong and the gap at A_2 and A_5 is large, the Bragg reflection can dominate the dynamics, forbidding the atoms from tunneling from the F band to the D band. Instead, the atoms at A_2 ($-3\hbar k_L$) will transfer completely to

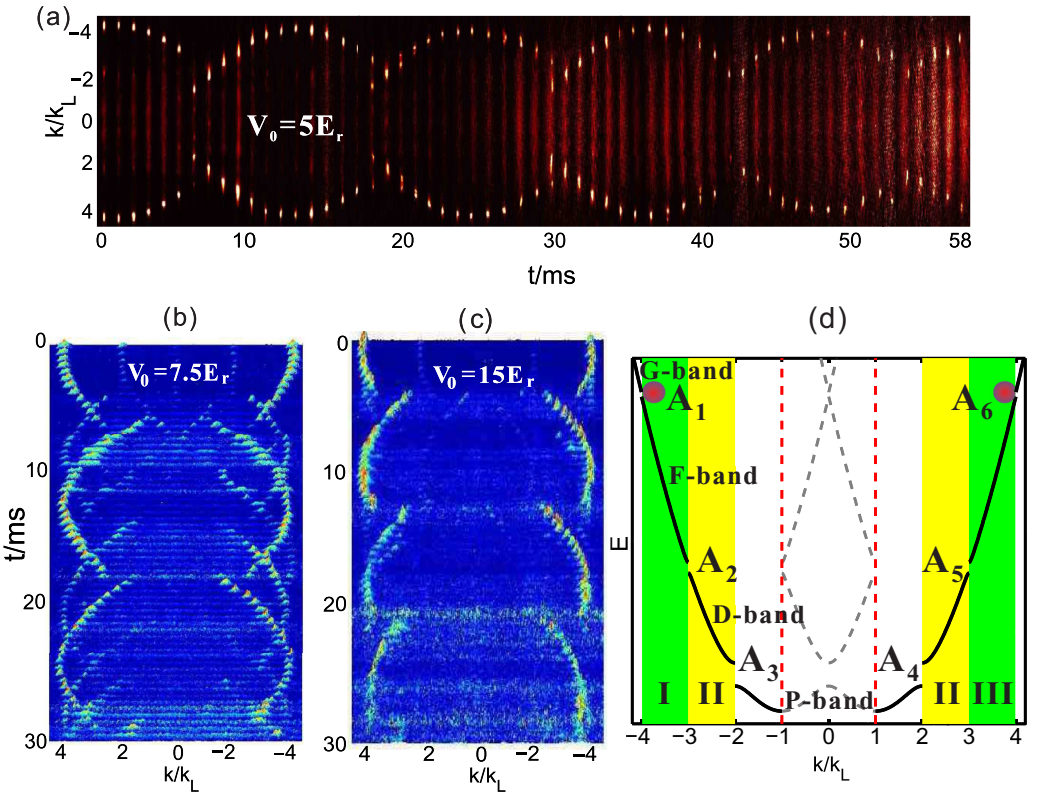

FIG. 2. Quantum oscillations of the BEC in higher bands of the OL. Experimental results in momentum space with (a) lattice depth $V_0 = 5E_r$, (b) $V_0 = 7.5E_r$, and (c) $V_0 = 15E_r$. The oscillations in (a) are across both the F and D bands, and oscillations in (c) are only within the F band; the dynamics in (b) are a superposition of the oscillations in (a) and (c). (d) Schematic of extended Bloch bands (P, D, F, and G) of a one-dimensional OL. The green areas (I and III) are for the F band, and the yellow areas (II) are for the D band.

A_5 ($3\hbar k_L$) via Bragg reflection, while the atoms at A_5 will also transfer completely to A_2. In this way, the quantum dynamics is confined within the F band. These oscillations only within the F band are observed in our experiment for $V_0 = 15E_r$ and are shown Fig. 2(c) with a period of 17 ms.

When the lattice strength is intermediate, the Bragg reflection at A_2 and A_5 will be partial: one part of the atoms will be reflected and undergo oscillations within the F band; the other part of the atoms will tunnel to the D band and oscillate across both the F and D bands. As a result, we should be able to observe a superposition of the two kinds of oscillations: across both the F and D bands and only within the F band, when the lattice is at an intermediate strength. This is indeed what we observed in experiment, as shown in Fig. 2(b), and simulated in theory, as shown in Figs. 3(c) and 3(d) for $V_0 = 7.5E_r$, where the two kinds of oscillations are clearly seen and the ratios of atoms undergoing the two different oscillations can be tuned by the lattice strength.

IV. THE THEORETICAL EXPLANATION AND SIMULATION

We have simulated the experiment with the one-dimensional time-dependent Gross-Pitaevskii equation (GPE) with interatomic interaction. In the simulation, the initial state is $\psi(x,t=0) = \psi_g(x)\phi_{q=0}(x)$, where $\psi_g(x)$ is the ground state of the BEC in a harmonic trap and $\phi_{q=0}(x)$ is the Bloch wave function in the G band at $q = 0$. We have plotted our numerical results in both real space and momentum space in Fig. 3 for $V_0 = 5E_r$ and $V_0 = 7.5E_r$. The results in momentum space agree well with the experimental results in Fig. 2. We can infer from Fig. 3(b) that the BEC can move away from the center of the trap by up to ± 100 μm for the oscillations in both the F and D bands. For oscillations in the F band, our numerical results indicate that this displacement can be up to ± 75 μm, which is much larger than what was observed in super-Bloch oscillations in Ref. [6]. There is a small discrepancy between the theoretical results and the experimental results. For example, there is a slight offset in the experimental oscillations around 6–7 ms for $V_0 = 5E_r$; this slight offset is not seen in the corresponding theoretical results. The explanation for this small discrepancy becomes clear when we discuss Bragg reflection in the next section.

It is difficult to observe oscillations in real space in experiment. To do that, we need to keep the TOF very short. Within such a short TOF, the atomic cloud is still very dense, and the TOF image is not proportional to the cloud density. At the same time, because of the short TOF, a large cloud of thermal atoms that have no time to disperse concentrates in the middle and obscures the TOF images.

As the BEC density profile varies smoothly over hundreds of lattice sites, its dynamics can be well described by the semiclassical dynamics of Bloch particles [22], where

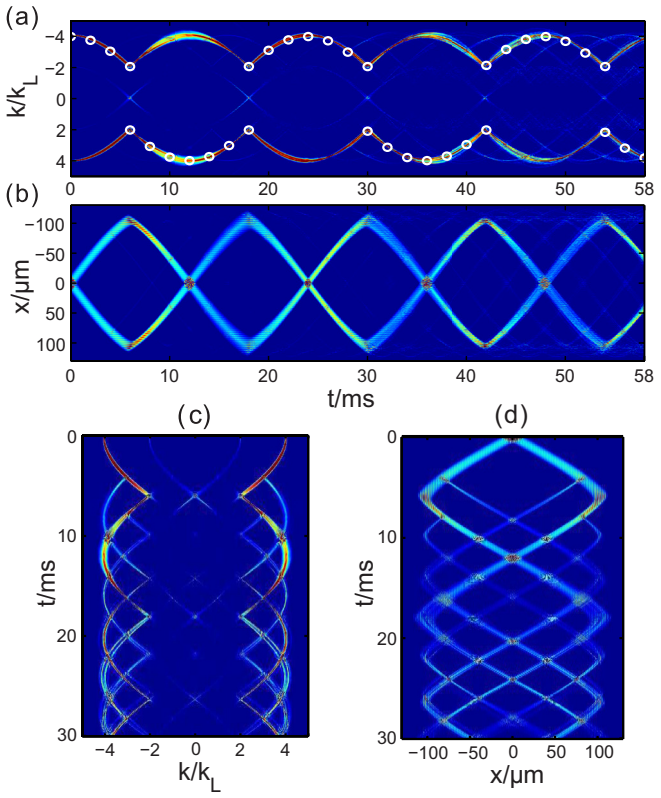

FIG. 3. The numerical simulations of quantum dynamical oscillations for the BEC in higher bands in both real space and momentum space. (a) and (b) Results for $V_0 = 5E_r$ and (c) and (d) results for $V_0 = 7.5E_r$. All theoretical results except for the white circles in (a) are from the GPE with interaction, while the white circles in (a) are from the semiclassical model without interaction.

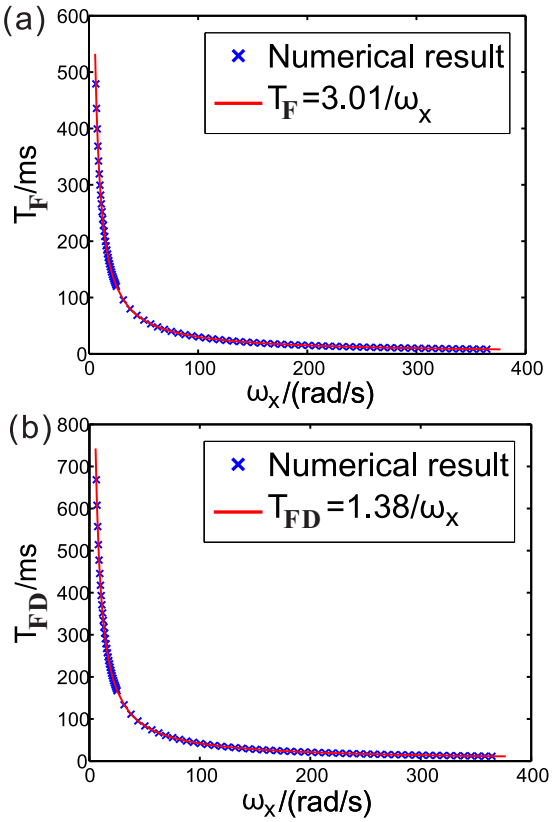

FIG. 4. The periods of the two kinds of oscillations for (a) $T_{\rm F}$ for $V_0 = 15E_r$ and (b) $T_{\rm FD}$ for $5E_r$. The red lines are fitting functions: (a) $T_{\rm F} = 3.01/\omega_x$ and (b) $T_{\rm FD} = 1.38/\omega_x$.

interaction is ignored,

$$\hbar\frac{d\boldsymbol{r}}{dt} = \nabla_{\boldsymbol{q}} E_n(\boldsymbol{q}), \tag{1}$$

$$\hbar\frac{d\boldsymbol{q}}{dt} = \boldsymbol{f}(\boldsymbol{r}), \tag{2}$$

where $E_n(\boldsymbol{q})$ is the nth energy band and $\boldsymbol{f}(\boldsymbol{r})$ is the force acting on the Bloch particle. For Bloch electrons in traditional condensed-matter physics, we usually have $\boldsymbol{f}(\boldsymbol{r}) = -e\boldsymbol{E} - e\frac{d\boldsymbol{r}}{dt} \times \boldsymbol{B}$. In our case, $\boldsymbol{f}(\boldsymbol{r}) = -m\omega_x^2 x\hat{e}_x$, with the harmonic trap frequency ω_x.

For simplicity, we describe the energy bands with a cosine function as $E_n(q) = A_n + \frac{B_n}{2}\cos(q\pi/k_L)$, with $n = F, D$ representing the F and D bands, respectively, and $|B_n|$ being the width of the energy bands. For this simplified case, we can solve Eqs. (1) and (2) analytically and find that the oscillation periods are

$$T_{\rm F} = \frac{4\hbar k_L}{\sqrt{m}\omega_x\pi}\frac{C_1}{\sqrt{B_{\rm F}}} \tag{3}$$

and

$$T_{\rm FD} = \frac{4\hbar k_L}{\sqrt{m}\omega_x\pi}\left(\frac{C_1}{\sqrt{B_{\rm F}}} + \frac{C_2}{\sqrt{-B_{\rm D}}}\right), \tag{4}$$

where $C_1 = \int_{q_+}^{k_L} \frac{{\rm d}(qa)}{\sqrt{\cos(q+a)-\cos(qa)}}$ and $C_2 = u\mathbf{K}(u)$. q_+ is the initial quasimomentum considering the finite size of the BEC, $u = (\frac{B_F}{-B_D}\cos^2\frac{q_+a}{2} + 1)^{-1/2}$, and $\mathbf{K}(u)$ is the complete elliptic integral of the first kind as $\mathbf{K}(u) = \frac{\pi}{2}\{1 + \sum_{n=1}^{+\infty}[\frac{(2n-1)!!}{2^n n!}]^2 u^{2n}\}$. It is obvious that the periods for the two kinds of oscillations are inversely proportional to ω_x.

This inverse relation does not change even when we use the realistic Bloch bands instead of the idealized cosine form. This is confirmed by our numerical results with the semiclassical equations (1) and (2), as shown in Fig. 4. Since $\omega_x = 2\pi \times 28$ Hz in our experiment, we have $T_{\rm F} = 17.1$ ms for $V_0 = 15E_r$ and $T_{\rm FD} = 23.9$ ms for $V_0 = 5E_r$, which agree very well with the experimental results in Fig. 2. In Fig. 3(a), the semiclassical oscillations are plotted as white circles, matching both the experimental result and the numerical GPE result.

V. HIGH-ORDER BRAGG REFLECTION

Bragg reflection (or scattering) at the Bloch band edge or center is a fundamental quantum process in periodic systems. As we have already seen, it plays a crucial role in the oscillations observed in our experiments. We now take a closer look at it by recording the absorption images every 0.1 ms. Two series of images are shown in Fig. 5, where we see clearly the reflection process between $\pm 3\hbar k_L$ in Fig. 5(a) under $15E_r$ and between $\pm 2\hbar k_L$ in Fig. 5(b) under $5E_r$. Bragg reflections have been demonstrated in lower bands with ultracold [1,23,24] atomic gases and in higher bands with ultracold atoms by using a time-dependent OL in Ref. [25], where only reflection results

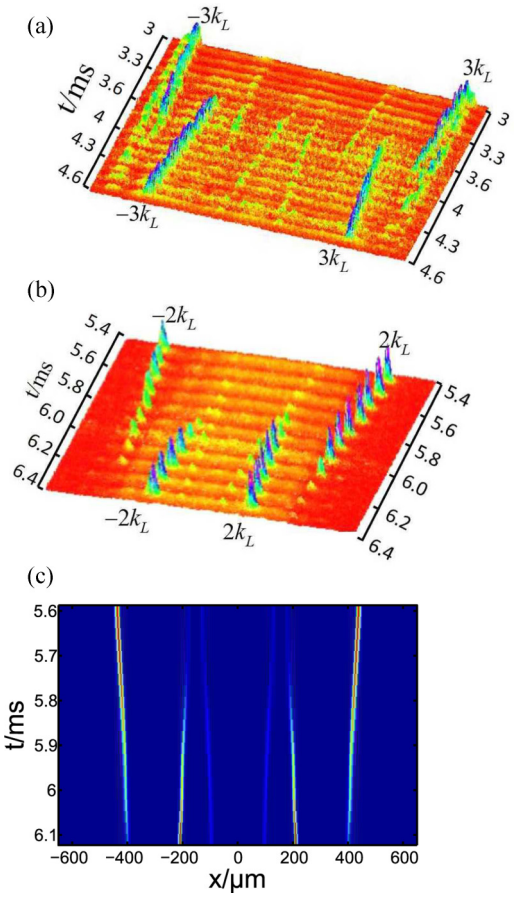

FIG. 5. High-order Bragg reflections process observed (a) at the edge of the F band for $V_0 = 15E_r$ and (b) at the center of the D band for $V_0 = 5E_r$ in the FBZ. (c) The simulation result from the GPE for $V_0 = 5E_r$. The vertical axis is the holding time t.

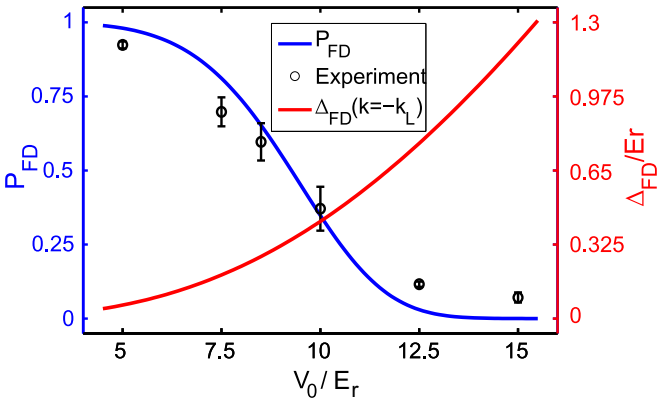

FIG. 6. The calculated transition probability from the F band to D band versus V_0 is shown as the blue solid line. The black circles are the experimental results. The band gaps between the F and D bands at the FBZ edge versus the lattice depth are also shown by the red solid line.

were given but the reflection processes were not shown. In our experiment, the processes of high-order Bragg reflections are obviously observed.

We use Fig. 5(b) to show in detail what is observed in our experiment. The Bragg reflection occurs roughly between 5.8 and 6.1 ms. During this period, atoms around $2\hbar k_L$ get scattered to $-2\hbar k_L$, while atoms around $-2\hbar k_L$ get scattered to $2\hbar k_L$. As a result, there are two fractions of atoms at $2\hbar k_L$: one fraction waits to be reflected to $-2\hbar k_L$, and the other consists of atoms just scattered from $-2\hbar k_L$. As atoms at $\pm 2\hbar k_L$ are located in different places, these two fractions at $2\hbar k_L$ are separated in coordinate space. With a 28-ms TOF, these two fractions appear as two different peaks. There are also two fractions for $-2\hbar k_L$. That is why atoms with the same momentum have different positions. The same is true for the reflection between $\pm 3\hbar k_L$ in Fig. 5(a). The experiment for $V_0 = 5E_r$ is simulated with the GPE. The computed density distributions in real space after a period of OL holding time t and a 28-ms TOF are shown in Fig. 5(c), which is consistent with our experimental result in Fig. 5(b).

When the atoms are not Bragg reflected, they tunnel from one band to a neighboring band. This is the well-known LZ tunneling. In other words, the Bragg reflection can be described as a process complementary to the LZ tunneling. Between the F and D bands, the tunneling is determined by $P_{\mathrm{FD}} = e^{-2\pi\gamma_{\mathrm{FD}}}$ [26], with

$$\gamma_{\mathrm{FD}} = \frac{\Delta_{\mathrm{FD}}^2}{4\hbar}\left|\frac{6\hbar k_L f(x)}{m}\right|^{-1}. \tag{5}$$

The calculated probability P_{FD} versus V_0 is shown in Fig. 6 by the blue solid line. It is clear that the tunneling probability decreases with the increasing lattice depth. It is close to 1 at $V_0 = 5E_r$ but close to zero at $15E_r$. Black circles are experimental results for the ratio of atoms that tunneled to the D band. There is very good agreement between the experiment and the theory. The band gaps Δ_{FD} between the F and D bands at quasimomenta $\pm\hbar k_L$ versus V_0 are shown by the red solid line in Fig. 6 to assist with the understanding of this quantum transition.

VI. CONCLUSION

In summary, we have loaded a BEC in a one-dimensional OL nonadiabatically into the G band. The BEC is then observed to tunnel to the F band and undergoes quantum oscillations within the F and D bands. The variable force exerted on atoms enables direct visualization of oscillations in higher bands in the momentum space. By controlling the Bragg reflection at the edges of the F and D bands with the OL, we have observed three different types of quantum oscillations. At weak lattice strength, oscillations between both the F and D bands are observed; at strong lattice strength, oscillations only within the F band are observed. At intermediate strength, a superposition of the above two dynamical oscillations is observed. Furthermore, we have directly demonstrated the high-order Bragg reflections process in high excited bands of the OL.

ACKNOWLEDGMENTS

We thank W. V. Liu and Q. Zhou for helpful discussions. This work is supported by the National Key Research and Development Program of China, under the National Key Basic Research Program (Grants No. 2016YFA0301501 and No. 2011CB921501) and the NSFC (Grants No. 61475007, No. 11334001, and No. 91336103).

[1] M. Ben Dahan, E. Peik, J. Reichel, Y. Castin, and C. Salomon, Phys. Rev. Lett. **76**, 4508 (1996).
[2] O. Morsch, J. H. Müller, M. Cristiani, D. Ciampini, and E. Arimondo, Phys. Rev. Lett. **87**, 140402 (2001).
[3] M. Cristiani, O. Morsch, J. H. Müller, D. Ciampini, and E. Arimondo, Phys. Rev. A **65**, 063612 (2002).
[4] M. Gustavsson, E. Haller, M. J. Mark, J. G. Danzl, G. Rojas-Kopeinig, and H.-C. Nägerl, Phys. Rev. Lett. **100**, 080404 (2008).
[5] M. Fattori, C. D'Errico, G. Roati, M. Zaccanti, M. Jona-Lasinio, M. Modugno, M. Inguscio, and G. Modugno, Phys. Rev. Lett. **100**, 080405 (2008).
[6] E. Haller, R. Hart, M. J. Mark, J. G. Danzl, L. Reichsöllner, and H. C. Nägerl, Phys. Rev. Lett. **104**, 200403 (2010).
[7] Q. Niu, X. G. Zhao, G. A. Georgakis, and M. G. Raizen, Phys. Rev. Lett. **76**, 4504 (1996).
[8] B. Wu and Q. Niu, Phys. Rev. A **61**, 023402 (2000).
[9] J. Liu, L. Fu, B. Y. Ou, S. G. Chen, D. I. Choi, B. Wu, and Q. Niu, Phys. Rev. A **66**, 023404 (2002).
[10] O. Zobay and B. M. Garraway, Phys. Rev. A **61**, 033603 (2000).
[11] B. M. Breid, D. Witthaut, and H. J. Korsch, New J. Phys. **8**, 110 (2006).
[12] Y. Mizumoto and Y. Kayanuma, Phys. Rev. A **88**, 023611 (2013).
[13] L. K. Lim, J. N. Fuchs, and G. Montambaux, Phys. Rev. Lett. **108**, 175303 (2012).
[14] F. Dreisow, A. Szameit, M. Heinrich, T. Pertsch, S. Nolte, A. Tünnermann, and S. Longhi, Phys. Rev. Lett. **102**, 076802 (2009).
[15] T. Uehlinger, D. Greif, G. Jotzu, L. Tarruell, T. Esslinger, L. Wang, and M. Troyer, Eur. Phys. J. Spec. Top. **217**, 121 (2013).
[16] G. Ritt, C. Geckeler, T. Salger, G. Cennini, and M. Weitz, Phys. Rev. A **74**, 063622 (2006).
[17] S. Kling, T. Salger, C. Grossert, and M. Weitz, Phys. Rev. Lett. **105**, 215301 (2010).
[18] S. Longhi, Europhys. Lett. **76**, 416 (2006).
[19] Y. Y. Zhai, X. G. Yue, Y. J. Wu, X. Z. Chen, P. Zhang, and X. J. Zhou, Phys. Rev. A **87**, 063638 (2013).
[20] X. X. Liu, X. J. Zhou, W. Xiong, T. Vogt, and X. Z. Chen, Phys. Rev. A **83**, 063402 (2011).
[21] D. Hu, L. X. Niu, B. G. Yang, X. Z. Chen, B. Wu, H. W. Xiong, and X. J. Zhou, Phys. Rev. A **92**, 043614 (2015).
[22] N. W. Ashcroft and N. D. Mermin, *Solid State Physics* (Saunders, Philadelphia, 1976).
[23] M. Kozuma, L. Deng, E. W. Hagley, J. Wen, R. Lutwak, K. Helmerson, S. L. Rolston, and W. D. Phillips, Phys. Rev. Lett. **82**, 871 (1999).
[24] R. Zhang, R. E. Sapiro, N. V. Morrow, R. R. Mhaskar, and G. Raithel, Phys. Rev. A **77**, 063615 (2008).
[25] S. J. Park, H. K. Andersen, S. Mai, J. Arlt, and J. F. Sherson, Phys. Rev. A **85**, 033626 (2012).
[26] C. Zener, Proc. R. Soc. London, Ser. A **137**, 696 (1932).